Energy Reports 7 (2021) 2821–2835

Contents lists available at ScienceDirect

Energy Reports

journal homepage: www.elsevier.com/locate/egyr

Research paper

Experimental analysis of hollow fiber membrane dehumidifier system with $SiO_2/CaCl_2$ aqueous desiccant solution

Yaping Wang [a,*], Behrooz Ruhani [b,*], Mohammad Ali Fazilati [c], S. Mohammad Sajadi [d,e], As'ad Alizadeh [f,g], Davood Toghraie [c]

[a] School of Materials Science and Engineering, Southeast University, Nanjing 211189, China
[b] Department of Mechanical Engineering, Najafabad Branch, Islamic Azad University, Najafabad, Iran
[c] Department of Mechanical Engineering, Khomeinishahr Branch, Islamic Azad University, Khomeinishahr, Iran
[d] Department of Nutrition, Cihan University-Erbil, Kurdistan Region, Iraq
[e] Department of Phytochemistry, SRC, Soran University, KRG, Iraq
[f] Department of Mechanical Engineering, Urmia University, Urmia, Iran
[g] Department of Mechanical Engineering, College of Engineering, University of Zakho, Zakho, Iraq

ARTICLE INFO

Article history:
Received 16 February 2021
Received in revised form 2 May 2021
Accepted 11 May 2021
Available online 17 May 2021

Keywords:
Hollow fiber membrane contactor system
Calcium chloride/silica desiccant solution
Sensible effectiveness
Latent effectiveness
Total effectiveness
2nd law efficiency

ABSTRACT

The liquid desiccant air conditioning system is amongst the promising technologies for the provision of efficient air conditioning, particularly in hot humid climate conditions. By their benefits, membrane-based dehumidification systems have drawn large attention. Various techniques are used to enhance the performance of different dehumidification system types. The effect of using calcium chloride nanofluid solution with the added silicate nanoparticles as a desiccant solution in a hollow fiber membrane contactor system investigated experimentally. The airflow rate through the fibers is 11.2 m^3/h with inlet relative humidity and temperature of 60 % and 35 °C, respectively. The sensitivity analysis was made to reveal the effect of desiccant temperatures, nanoparticle concentrations, and solution flow rates on sensible, latent, and total effectiveness and 2nd law efficiency of the system. The results indicate that using nanofluid instead of a pure desiccant solution, the values of sensible and latent effectiveness improved at the condition of high inlet solution temperature. The effect of employing nanofluid on exergy performance is the highest for the highest concentration of nanoparticles and inlet solution temperature. The maximum change of exergy destruction rate resulted by using nanofluid solution took place at a maximum flow rate of 244 ml/min for 1% nanofluid concentration. Using 1 % nanofluid instead of a pure solution, the rate of exergy destruction increased by 82 % and 160 % for 20 °C and 26 °C solution temperatures, respectively.

1. Introduction

People spend most of their living time inside the buildings (Huang et al., 2012). The increasing standards of living and the resulted high demand for thermal comfort have drawn the large attention of researchers for developing efficient Air Conditioning (*AC*) systems. Presently, Vapor Compression Cooling Systems (*VCSs*) are developed as *AC* systems that deal with both the latent and sensible loads of buildings. These systems which are characterized by heavy dependence on electrical energy, have limited efficiency in dealing with latent loads (Wen and Lu, 2019). In this way, desiccant air conditioning systems have been introduced as a replacement for *VCSs* (Abdel-Salam and Simonson, 2016). In these systems, absorber and regenerators are the main components, and their Heat And Mass Transfer (*HMT*) characteristics directly affect the system performance (Fazilati et al., 2017). The contact type between the Liquid Desiccant (*LD*) and air streams could be in direct or indirect forms (Fazilati et al., 2016). Qi et al. (2020) reviewed the liquid dehumidification systems considering the optimization methods for improving the system performance. They reviewed the optimization methods of dehumidifiers/regenerators, hybrid systems, and material optimization including desiccants and membrane materials, and modifications of packing/plate surfaces. Through recent decades, different Heat And Mass Transfer (*HMT*) techniques have been introduced and applied to improve the performance of air dehumidification systems; using the natural convection *H/M* loop (Yan et al., 2020), applying the hydrophilic coating on contact surfaces (Dong et al., 2017a) and the addition of surfactant (Lin and Shigang, 2011) or nanoparticles (*NPs*) (Pang et al., 2015) are amongst the employed techniques.

* Corresponding authors.
E-mail addresses: abcwangyaping@live.com (Y. Wang), b.ruhani55@gmail.com (B. Ruhani).

https://doi.org/10.1016/j.egyr.2021.05.010

Nomenclature

a	activity coefficient
A	area (m^2)
AC	air conditioning
AHRI	American heating and refrigerating institute
ASTM	American society for testing and materials
C	concentration (kg_{salt}/kg_{sol})
CaCl2	calcium chloride
cp	specific heat capacity (kJ/kg °C))
$\overline{c}_p$	specific heat capacity (kJ/kmol °C))
Cr*	specific heat ratio
Cu	copper
d1	inner diameter (m)
d2	outer diameter (m)
DLS	dynamic light scattering
EES	engineering equation solver (computer software)
F	nanoparticles concentration
G	mass flow rate (kg/s)
h	specific enthalpy (kJ/kg)
H	enthalpy (kJ)
H/M	heat and mass
HFM	hollow fiber membrane
HFMEE	hollow fiber membrane energy exchanger
HMT	heat and mass transfer
HR	humidity ratio (gr/kg)
LAMEE	liquid to air membrane energy exchanger
LDAC	the liquid desiccant air conditioning system
LD	liquid desiccant
LDS	liquid desiccant system
LiBr	lithium bromide
LMTD	log mean temperature difference
m	molality of solution (mol/kg)
M	molar mass (kg/kmol)
MRR	moisture removal rate (kg/s)
MWNT	multi-walled nanotube
$\dot{m}$	mass flow rate (kg/s)
NF	nanofluid
NP	nanoparticle
NTU	number of the transfer unit
p	pressure (kPa)
PVP	polyvidone
PVDF	PolyVinylidene fluoride
PTFE	Poly tetra fluoro ethylene
$\dot{Q}$	heat transfer rate (W)
R	gas constant (kJ/kg K)
$\overline{R}_u$	universal gas constant (kJ/kmol K)
SHF	rate of heat transfer (W)
SiO_2	silicon dioxide
t	time (s)
T	temperature (K)
TEG	tri-ethylene glycol
VCS	vapor compression system
$\dot{V}$	volume flow rate (m^3/h)
wt	weight
x	mole fraction
X	exergy (kJ)
XRD	X-ray diffraction

Greek symbols

Δ	difference
ϵ	effectiveness
φ	the volume fraction of nanoparticle
γ	molal activity coefficient
μ	chemical potential
ν	disassociation number
ρ	density (kg/m^3)

Subscripts

0	ultimate dead state
1	inlet flow, the initial state
2	outlet flow, the final state
a	air
bf	base fluid
db	dry bulb
des	destroyed
e	empty
eq	equilibrium
fg	liquid to gas
ha	humid air
i	inlet flow
l	latent
L	length (m)
$\dot{m}$	mass flow rate (kg/s)
max	maximum
mem	membrane
min	min
nf	nanofluid
o	outlet flow
p	pressure (kPa)
s	sensible, solute
sol	desiccant solution
t	total
v	water vapor
w	liquid water
wb	water vapor

Superscripts

*	restricted dead state
0	Standard chemical potential
±	ions mean quantity of the electrolyte
–	molar quantity

The effects of using the additives have been studied on surface wettability (Wen et al., 2018c) and causticity on the metals (Wen et al., 2018b). The studies on the effect of using *NP* on the saturated vapor pressure of *NF*s are very limited; in this field, the works of Tso and Chao (2015) and Zhu et al. (2011) could be mentioned. Zhu et al. (2011) studied the effect of Al_2O_3 NP on the thermo-physical properties of water. The results show that the *NP* volume concentration increases the thermal conductivity, viscosity, and saturation vapor pressure, where it decreases the latent heat of vaporization and surface tension. Tso and Chao

(2015) studied saturated vapor pressure, enthalpy of evaporation, and evaporation rate of aqueous *NF* solutions of Al_2O_3 and TiO_2 with concentrations of 0.01% to 2% and particle sizes of 13 nm-80 nm. It is found that increasing the *NP* concentration decreases the evaporation enthalpy.

The effects of using NF desiccant solutions are focused mainly to direct dehumidification systems. Ali et al. (2003) studied the performance of an internally cooled/ heated flat-plate dehumidifier/regenerator with an aqueous solution of $CaCl_2$ with *Cu*-ultrafine particles. Their numerical results showed the little improving effect of adding NPs on *HMT* characteristics of the system which was attributed to little thickness of the desiccant film. The dehumidification characteristics of aqueous solutions of *LiCl* with the combined additive of Polyvinyl Pyrrolidone (*PVP*) surfactant and Multi-Walled Carbon Nanotubes (*MWNT*s), and with *PVP* surfactant only in a flat-plate internally cooled dehumidifier was investigated by Wen et al. (2018c). The results showed the moisture absorption improvement up to 26.1% and 25.9% for desiccants with Polyvinyl Pyrrolidone (*PVP*) surfactant only and with surfactant and the *MWNT*s, respectively. As an essential tool for analyzing the performance of the dehumidification system, the exergy and 2nd law efficiency could be used. Based on the authors' knowledge, the studies on evaluating the air dehumidifier systems using the exergy analysis are very limited. Yulin Ma et al. (2020) analyzed the natural convection *HMT* loop from the energy and exergy viewpoints. The inlet air flow rate was the variable parameter and the 2nd law efficiency was reduced by the inlet air flow rate increase to system. By the exergy analysis and the 2nd law of thermodynamics, Xiong et al. (2010) proposed a two-stage liquid desiccant dehumidification system. By the exergy analysis of the basic and two-stage systems, they showed that the exergy loss in desiccant–desiccant heat recovery system could be decreased by increasing the concentration difference between the strong and weak desiccant solutions. Zhang et al. (2014) showed that the selection of the dead state is a key parameter for analyzing the exergy performance of these systems. The studied system was the falling film dehumidification type with *LiBr* desiccant solution and they demonstrated that reducing the exergy destruction improves *COP* of the system.

As the indirect contact dehumidification type system, membrane systems have drawn large attention through recent years (Yulin Ma et al., 2020). Hollow Fiber Membrane (*HFM*) contactor systems with their advantages such as the large per unit volume of contact areas (up to 2000 m^2/m^3) have a position above other similar membrane contactor systems. The employed membrane, as the air/liquid contactor for air dehumidification, separates two neighboring fluid phases. For the desiccant solution of aqueous type, the mechanism of air dehumidification is by penetrating the vapor from the gas to the desiccant side through the membrane surface, and in this process, the water transfer in liquid form should be banned. By this, as the major property, the membrane should be hydrophobic and this property comes firstly from its material. After, the pore size (reported by mean pore size) and the fiber diameter are the next important HFM specifications. To avoid the risk of pore wetting of membrane in conjunction with liquid desiccant dehumidifiers, the membrane surface should be hydrophobic. Some materials are inherently hydrophobic and some are made hydrophobic through chemical techniques; Polypropylene (PP) and Poly Tetra Fluoro Ethylene (PTFE) are the instances of the former and Polyvinylidene Fluoride (PVDF) is the instance of the latter group. Sometimes the membrane surface is coated with other materials to repel the water molecules (Qi et al., 2020). Shadanfar et al. (2021) investigated the air dehumidification in the HFM system using nanofluids of tri-ethylene glycol with carbon nanotubes, silica, and aluminum oxide with different weights percent. The results show that the air dehumidification is the highest for CNT nanofluid and SiO_2 and Al_2O_3 stand in the next stages. Liu et al. (2020) studied the air dehumidification using the PVDF hollow fiber membrane whose outer surface modified with poly Vinyl Alcohol (PVA) and Poly Dopamine (PDA). The results show the three layer PDA–PVA/PVDF surface with PDA significantly enhanced the dehumidification performance.

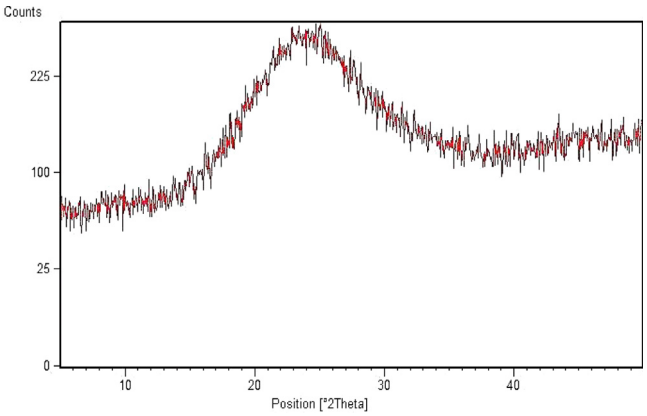

Fig. 1. The output diagram of *the XRD* test.

Based on the authors' knowledge, the studies on the effect of using *NF* desiccant on *HMT* characteristics of dehumidifiers are mainly in direct contact systems; also, considering the very little works on *NF* desiccant properties, including the vapor pressure, activation energy, etc. which are required to determine the exergy values of *NF*, a literature gap was found in exergy analysis of dehumidification in *HFM* systems with *NF* desiccant. As the first step toward the application of aqueous NF solution of $CaCl_2$ in *HFM* dehumidification systems and assessing its energy and exergy performance, dehumidification properties of $CaCl_2/H_2O$-SiO_2 desiccant solution in a Hollow Fiber Membrane Energy Exchanger (*HFMEE*) investigated experimentally. The airflow is directed into the fibers while desiccant flows over the fibers in the shell and tube *H/M* exchanger. Different types of effectiveness values including the sensible, latent and total effectiveness, Sensible Heat Factor (*SHF*) and 2nd law efficiency were analyzed as the energy and exergy characteristics of system. The sensitivity analysis was performed to unveil the effect of *NF* concentration, its temperature, and flow rate on the system performance. In the next section, after the explanation of the experimental setup and its components, the procedures and the operating conditions are described. The results are given next in the results and discussion section and finally, the conclusion is drawn.

2. The system description, methodology, and the validation

In this study, an aqueous solution of $CaCl_2$ with ultrafine particles of SiO_2 in volume percent of 0, 1%, and 2% adopted as the *NF* desiccant solution. The solution is prepared by the two-step method and the final solution is examined by the *XRD* test, whose output diagram is depicted in Fig. 1. The two-step method of NF preparation method is most appropriate and economical for the production of aqueous NF of metal oxides (Kim et al., 2012). Here, the solution is subjected to the cavitation bubbles in the pressurized vessel called reactor; next by increasing the pressure, the NPs are added to the solution slowly. The diagram and locations of the peak values approve the amorphous form of used NPs and their high purity. Amorphous materials, like glass, do not produce sharp diffraction peaks. Also, the *DLS* test shows the mean diameter of particles to be 23.32 nm. The stability of *NF*

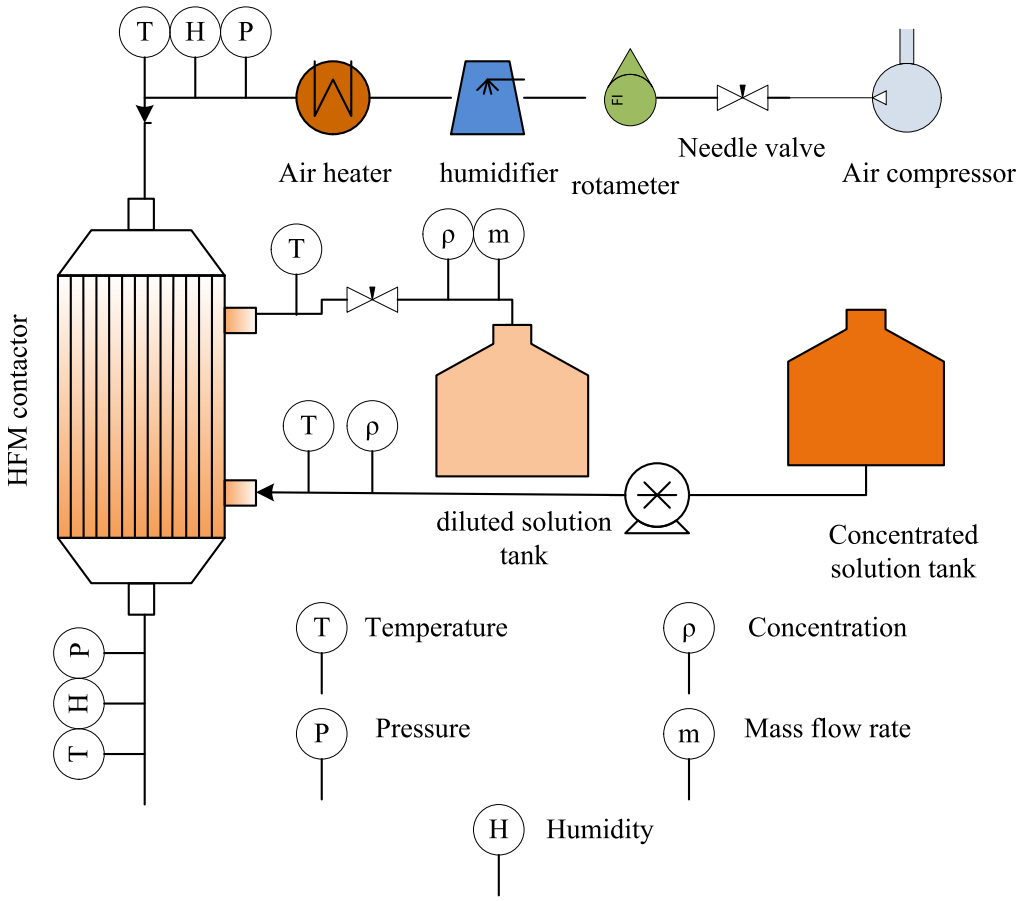

Fig. 2. The schematic of the system setup including the air compressor, humidifier, air heater, HFM contactor, the diluted and concentrated solution tanks, the controllers, and the measurement sensors.

was examined by investigating the samples in periods of 7 days and a month, which show no settlement or agglomeration during this time.

The setup system, whose schematic is shown in Fig. 2, has three main subsystems; the *HFMEE*, the air, and the solution processing systems. The measurement devices get data from the fluid streams via their sensors located in the air and desiccant flow paths.

The *HFMEE* is similar to a shell and tube heat exchanger, where *HFM*s are in place of the tubes. The air flows into the fibers and the solution stream is in the shell side over the fibers. The fibers are made up of *PVDF*, whose inside diameter is 640 μm and are provided by the national company. The schematic of the module and specifications of the fibers and the exchanger shell are shown in Fig. 3 and Table 1, respectively.

The flow rate and pressure of the processing air are regulated utilizing a needle valve and pressure regulator, respectively. Also, the value of the airflow rate is determined using a calibrated rotameter. The humidity and temperature of the processing air set to specified values by regulating the air heater and humidifier systems (Fig. A.1), respectively.

A handmade psychomotor is used by which the dry and wet bulb temperatures of the air could be determined (Fig. A.2). Also, the air pressure loss is determined using the glass U-tube manometer. By the same air flow rate through the experiments, the air pressure drop is not altered and its value was measured to be 160mmHg. The desiccant solution is pumped by a diaphragm pump from the concentrated solution tank into the shell side of the exchanger and after *HMT* is directed to the weak solution tank. Before connecting the air tube to the exchanger, its properties are adjusted in a process which is described in the appendix under Fig. A.3.

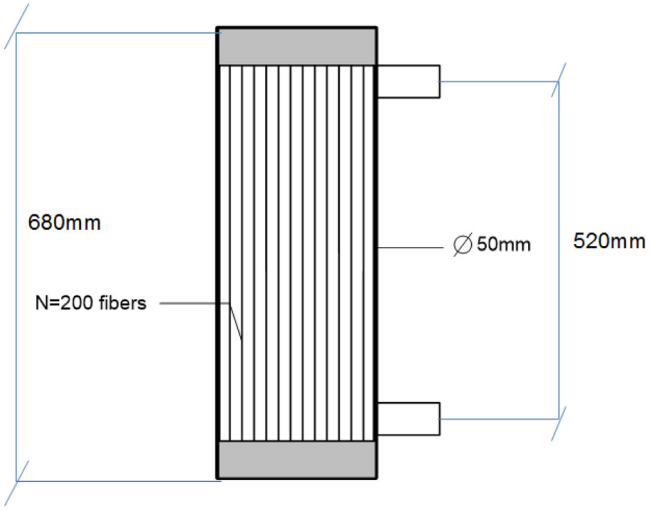

Fig. 3. The main dimensions of the module.

A set of experiments had been organized to unveil the effect of desiccant temperature, its flow rate, and NP concentration on the exergy and energy performance of the system. The properties of inlet air are selected according to values of *AHRI* summer air conditions and their values along with the solution and *NP* properties are listed in Table 2 (AHRI A, 2005). It is

Table 1
Specification of *HFM*s in the module.

Specification	Unit	Value
Membrane material	–	*PVDF*
Fibers inner diameter	μm	640
Fibers outer diameter	μm	1300
Membrane thickness	μm	330
Number of fibers in the exchanger	–	200
surface density in the exchanger	m^2/m^3	528
Cross sectional surface density	m^2/m^2	0.14
Mean pore size of fiber material	μm	0.03
Tortuosity of fiber material	–	3.82
The porosity of fiber material	–	0.55

worth noting that the *AHRI* provides the examination procedure for air dehumidification systems which is used for performance evaluation.

The values of outlet desiccant and air temperatures are got every 5 min; data acquisition goes on until the parameters got fixed vs. the time.

The flow rate of the desiccant solution is determined using the timer of the graduated cylinder. The air and solution temperature are measured using the standard *ASTM* calibrated glass thermometer and the steady-state concentration of desiccant solution determined by sampling and direct measurement. The samples are firstly weighted (w_1) and then, let to be dried by heating it and are weighed again (w_2). After, the concentration value is calculated as (w_2-w_e)/(w_1-w_e) where (w_e) is the weight of the empty container. The weighing is performed by a digital balance with an accuracy of 0.001 gr. Other thermodynamic properties of desiccant and air streams are determined by *EES* software using the corresponding values of temperature and concentration, dry and wet bulb temperatures, and pressure.

At steady-state, considering the adiabatic condition of *the H/M* exchanger, the heat and moisture conservation laws could be written as Eqs. (1) and (2) respectively;

$$G_{sol}(h_{sol,o} - h_{sol,i}) = G_a(h_{a,o} - h_{a,i}) \tag{1}$$

$$G_{sol}C_{sol,i}(\frac{1}{C_{sol,o}} - \frac{1}{C_{sol,i}}) = G_a(\omega_i - \omega_o) \tag{2}$$

The left side of Eqs. (1) and (2) demonstrates the transferred moisture and heat in solution and the right side declares the corresponding values in air, respectively. In Eqs. (1) and (2) *h*, *G*, and *C* refer to enthalpy, mass flow rate, and solution concentration, and *i*, *o*, *a*, and *sol* subscript stand for inlet and outlet flows, air, and the solution respectively. From the little change of solution concentration in the mass conservation equation, the energy conservation law stated by Eq. (1) was taken as a basis to determine the steady-state achievement. For verification of steady-state achievement, the maximum discrepancy of ±20% between the sides of energy equation relation was considered to take into account the data measuring uncertainties and also the small amount of heat transfer between the system and environment (Wen et al., 2018c,a; Dong et al., 2017b; Liu et al., 2015). After this, the experimental system would be approved for later investigations

3. Evaluation indexes

The *HFMEE* system is evaluated from the energy and exergy viewpoints. As the representatives of energy performance, system effectiveness values including the sensible, latent, and total effectiveness and Sensible Heat Factor (*SHF*) and as the exergy evaluation index, 2nd law efficiency would be used and are explained in the following subsections.

3.1. Effectiveness

Different forms of effectiveness are defined to demonstrate the moisture, sensible heat, and total heat transferability of the system which are usually denoted by latent, sensible, and total effectiveness, respectively. In energy exchanger systems the value of effectiveness (sensible and latent) depends mainly on two parameters; a number of a transfer unit or *NTU* (in its sensible as Eq. (3) or latent forms as Eq. (4)) and flow rate or heat capacitance ratio (Eqs. (6) and (7), respectively). The value of NTU_s is determined mainly by transfer coefficients in solution (h_{sol}) and air sides (h_a), but from the greater value of solution side coefficients and its reverse effect in sensible heat transfer coefficient (U_s in Eq. (5)), it is the airside transfer coefficient which primarily determines sensible transfer coefficients. A similar argument could be made about the latent transfer coefficient; in this way, the value of flow rate ratio (*R* in Eq. (6)) may be varied only by changing the solution flow rate and its effect studied on latent effectiveness. Therefore, to retain the values of sensible and latent *NTU* unchanged, the airflow rate was kept fixed and the other parameters i.e. flow rate ratio (Eq. (6)) and heat capacitance ratio (Eq. (7)) are varied by changing the solution flow rate. In Eqs. (3) to (7) the subscripts *s*, *l*, *min*, *sol*, and *a* refer to sensible, latent, minimum, solution and air streams and *A*, *U*, *L*, *h*, and $\dot{m}$ are surface contact area, overall transfer coefficient, exchanger length, enthalpy, and the mass flow rate, respectively.

$$NTU_s = \frac{U_s A}{(\dot{m}c_p)_{\min}} \tag{3}$$

$$NTU_L = \frac{U_l A}{(\dot{m})_{\min}} \tag{4}$$

$$U_s = \left[\frac{1}{h_{sol}} + \frac{\ln(d_2/d_1)}{2\pi L k_{mem}} + \frac{1}{h_a}\right]^{-1} \tag{5}$$

$$R = \frac{(\dot{m})_{sol}}{(\dot{m})_a} \tag{6}$$

$$Cr^* = \frac{(\dot{m}c_p)_{sol}}{(\dot{m}c_p)_a} \tag{7}$$

3.1.1. Sensible effectiveness

As a sensible heat exchanger device, sensible effectiveness specifies the capability of energy exchanger for transferring thermal energy in its sensible form (nominator of Eq. (8)) compared to its maximum possible value (denominator of Eq. (8));

$$\varepsilon_s = \frac{\dot{Q}_s}{\dot{Q}_{s,\max}} = \frac{(\dot{m}c_p)_a(T_{1,a} - T_{2,a})}{(\dot{m}c_p)_{\min}\Delta T_{\max}} \tag{8}$$

The "*min*" and "*max*" subscripts denote the minimum and maximum values which are chosen between the air and desiccant streams (Eq. (9)). Also, $\Delta T_{\max}$ is the maximum temperature difference between the air and desiccant (Eq. (10)).

$$(\dot{m}c_p)_{\min} = \min\left\{(\dot{m}c_p)_{sol}, (\dot{m}c_p)_a\right\} \tag{9}$$

Table 2
The operating conditions of the experiments.

Material	Parameter	Range
Solution	Concentration (wt%)	47
	Volume flow rate (ml/min)	(160–244)
	Inlet temperature (°C)	20–26
Process air	Inlet humidity ratio (gr/kg)	21.38
	Volume flow rate (m^3/h)	11.2
	Inlet temperature (°C)	35
SiO_2 *NPs*	Volumetric concentration (%)	0–2

$$\Delta T_{\max} = T_{\max} - T_{\min} \tag{10}$$

In Eq. (10), the maximum and minimum values of temperature are selected between the inlet and outlet temperatures of air and solution streams. The desiccant mass flow rate is determined by multiplying its volume flow rate to density, according to Eq. (11).

$$\dot{m}_{sol} = \rho_{sol} \times \dot{V}_{sol} \tag{11}$$

In Eq. (11), ρ_{sol} and $\dot{V}_{sol}$ stand for density and volume flow rate of desiccant, respectively. The density and specific heat values of *NF* desiccant are calculated based on their corresponding values for a pure desiccant solution, according to Eqs. (12) and (13), respectively (Xuan and Roetzel, 2000; Pak and Cho, 1998).

$$\rho_{nf} = \phi\rho_p + (1-\phi)\rho_{bf} \tag{12}$$

$$c_{p,nf} = \frac{(1-\phi)(\rho c_p)_{bf} + \phi(\rho c_p)_p}{(1-\phi)\rho_{bf} + \phi\rho_p} \tag{13}$$

In Eqs. (12) and (13), "ϕ" represents the volumetric concentration of NP in desiccant, and the subscript "*bf*" referred to the base fluid, which is the calcium chloride desiccant solution. The thermophysical properties of calcium chloride solution are determined using the correlations given by Conde (2004); also, the particle properties are obtained from the NP manufacturer (Nanomaterials, 2018).

3.1.2. Latent effectiveness

The latent effectiveness describes the moisture removal rate (*MRR*) (nominator of Eq. (14)) vs. the corresponding maximum possible value (denominator of Eq. (14));

$$\varepsilon_l = \frac{\dot{m}_v}{\dot{m}_{v,\max}} = \frac{\dot{m}_a(\omega_{a,i} - \omega_{a,o})}{\dot{m}_{\min}(\omega_{\max} - \omega_{\min})} = \frac{MRR}{MRR_{\max}} \tag{14}$$

In Eq. (14), ω is the air humidity ratio, and the subscripts *a*, *i*, *o*, and *v* denote the air, inlet–outlet, and vapor, respectively. The minimum value of mass flow rate is chosen between the air and solution streams, and the value of $\Delta\omega_{\max}$ is the difference between the maximum (Eq. (15)) and minimum (Eq. (16)) values of air humidity ratio.

$$\omega_{\max} = \max\left\{\omega_{a,i}, \omega_{a,o}, \omega_{a@(T_{sol,i},C_{sol,i})}, \omega_{a@(T_{sol,o},C_{sol,o})}\right\} \tag{15}$$

$$\omega_{\min} = \min\left\{\omega_{a,i}, \omega_{a,o}, \omega_{a@(T_{sol,in},C_{sol,i})}, \omega_{a@(T_{sol,o},C_{sol,o})}\right\} \tag{16}$$

For calculating the equivalent specific humidity of inlet desiccant ($\omega_{\min}$ in Eq. (14)), the vapor pressure over the desiccant surface (P_v) should be substituted in Eq. (17);

$$\omega_s = 0.622\frac{P_v}{P - P_v} \tag{17}$$

In the case of using pure calcium chloride solution, the equilibrium vapor pressure of desiccant is determined using the correlation of Conde (2004), which is based on the saturated vapor pressure of water. In the case of *NF* desiccant, due to collision and interaction between the particles and fluid, it is expected that the addition of NP affects the equilibrium saturated vapor pressure (Xuan and Li, 2000). As mentioned earlier in the Introduction, the studies about the effects of *NP* on the saturation vapor pressure of aqueous *NF* solution are very limited, and in the case of desiccant solutions, no report was found. The only existing studies in this field are the works of Zhu et al. (2011) and Tso and Chao (2015), which measured the saturation vapor pressure of water-based *NF* of Al_2O_3 and TiO_2 with particle sizes of 13 nm to 80 nm. Based on their results and for the particle size of 21 nm, a maximum vapor pressure reduction of 3.8% is observed for the investigated solution temperatures. Considering this fact and lack of any other works in the field, for determining vapor pressure of *NF* desiccant the saturation vapor pressure of aqueous *NF* proposed by Tso and Chao (2015) substituted in place of pure water saturation pressure in correlation of Conde (2004).

3.1.3. Total effectiveness

In energy exchanger systems, total effectiveness is used to express the system's ability to transfer total energy (sum of sensible and latent forms). The value of total effectiveness is the ratio of energy transfer rate (nominator of Eq. (18)) to the maximum possible one (denominator of Eq. (18));

$$\varepsilon_t = \frac{(H_{1,a} - H_{2,a})}{(H_{1,a} - H_{1,sol})} = \frac{(\dot{m})_a(h_{1,a} - h_{2,a})}{(\dot{m})_{\min}\Delta h_{\max}} \tag{18}$$

In Eq. (18), *H* and *h* represent the enthalpy and specific enthalpy and *1* and *2* subscripts referred to as inlet and outlet streams, respectively. The value of $\Delta h_{\max}$ in Eq. (18) was obtained by subtracting the minimum value of enthalpy from the maximum one whose values are determined between the enthalpies of engaged fluids i.e. air and desiccant solution (Eq. (19)). Considering different phases of air and desiccant, a common basis should be adopted for determining their enthalpies. This common basis is to use the air enthalpy which is in an equilibrium state with desiccant fluid in place of solution enthalpy whose value is determined by Eq. (20); the equilibrium state means having the same temperature and vapor pressure as desiccant fluid.

$$\Delta h_{\max} = h_{\max} - h_{\min} \tag{19}$$

$$h_a = c_{p,a}T_a + \omega \times (h_{fg} + c_{p,v}T_a) \tag{20}$$

The values of $h_{\max}$ and $h_{\min}$ in Eq. (19) are determined using Eqs. (21) and (22), respectively.

$$h_{\min} = \min\left\{h_{a,i}, h_{a,o}, h_{a@(T_{sol,i},\omega_{sol,i})}, h_{a@(T_{sol,o},\omega_{sol,o})}\right\} \tag{21}$$

$$h_{\max} = \max\left\{h_{a,i}, h_{a,o}, h_{a@(T_{sol,i},\omega_{sol,i})}, h_{a@(T_{sol,o},\omega_{sol,o})}\right\} \tag{22}$$

3.2. Sensible heat factor (SHF)

As a total energy exchanger, a parameter that may be used to compare its ability for transferring sensible and latent forms of thermal energy is the sensible heat factor or *SHF*. The *SHF* describes the rate of sensible (nominator of Eq. (23) to total heat transfer rate (denominator of Eq. (23).

$$SHF = \frac{\dot{Q}_s}{\dot{Q}_l + \dot{Q}_s} = \frac{\dot{m}_a c_p(T_{i,a} - T_{o,a})}{\dot{m}_a(h_{i,a} - h_{o,a})} \tag{23}$$

The value of *SHF* varies between 0 and 1; the smaller value of *SHF* shows a greater share of latent heat from total energy transfer, and vice versa, the larger *SHF* demonstrates that the larger portion of energy transfer is in the sensible form.

3.3. Exergy flow and 2nd law efficiency

Exergy is defined as the maximum useful work that could be gotten from a specified form of energy in a process that finally gets the system to an equilibrium state with the environment (Kotas, 2013). In the air dehumidification system, the equilibrium with a reference state includes mechanical, thermal, and chemical equilibrium for all the engaged flows, i.e., liquid desiccant and humid air (Bejan, 2016). For both liquid desiccant and humid air, the total exergy is the summation of thermal, mechanical, and chemical exergies. Considering the environment temperature and pressure as thermodynamics properties of dead state conditions, the total exergy rate of humid airflow could be determined by Eq. (24) (Bejan, 2016). In Eq. (24), T_0 and P_0 denote the dead state temperature and pressure, and the first two and last terms indicate the physical (thermomechanical) and chemical exergies of humid air, respectively.

$$X_{t,ha}(T,p,\omega) = \dot{m}_a \left\{ \begin{array}{l} (c_{p,a}+\omega c_{p,v})T_0\left(\frac{T}{T_0}-1-\ln\frac{T}{T_0}\right)+(1+1.608\omega_0)R_aT_0\ln\frac{p}{p_0} \\ +R_aT_0\left[(1+1.608\omega)\ln\frac{1+1.608\omega_0}{1+1.608\omega}+1.608\omega\ln\frac{\omega}{\omega_0}\right] \end{array} \right\} \quad (24)$$

The liquid desiccant is mainly an aqueous solution of calcium chloride, and the total molar exergy of such a two-component system (water and solute) could be determined by Eq. (25) (Zhang et al., 2014). The "*" subscript in Eq. (25) denotes the restricted dead state condition at which the system has thermo-physical equilibrium with the dead state, and its pressure and temperature are P_0 and T_o, respectively.

$$X_{t,sol}(T,p,x_s) = \frac{\dot{m}_{sol}}{M_{sol}}\left\{\overline{c}_{p,s}(T-T_0)-\overline{c}_{p,s}T_0\ln\frac{T}{T_0} + x_s(\mu_s{}^*-\mu_{0,s})+(1-x_s)(\mu_w{}^*-\mu_{0,w})\right\} \quad (25)$$

The first two terms of Eq. (25) indicate the physical exergy and the summation of the last two terms is the chemical exergy of desiccant flow; also, "x" and "M_{sol}" represent the mole fraction of species and molar mass of solution, respectively. The conversion of mass concentration to a molar fraction of solute (x_s) and water (x_w) is performed by Eqs. (26) and (27), respectively.

$$x_s = C\times\frac{M_{sol}}{M_s} \quad (26)$$

$$x_w = (1-C)\times\frac{M_{sol}}{M_w} \quad (27)$$

In Eqs. (26) and (27), M_s and M_{sol} are the solute and solution molecular mass; also, the value of M_{sol} depends on the mass concentration (C) and solute and water molecular masses, according to Eq. (28);

$$M_{sol} = C\times M_s+(1-C)\times M_w \quad (28)$$

By Eq. (25), the chemical exergy of the water and solute is determined using their potential chemical values. The chemical potential of solution components, i.e., solute and water, are functions of both activity coefficient and standard chemical potential (Pitzer, 1995). Since these properties are usually found in literature in terms of component molality (moles of solute per kilogram of solvent, i.e., water) (Rard and Clegg, 1997), the chemical potential of solute and water are presented based on solution molality, according to Eqs. (29) and (30), respectively.

$$\mu_s(T,p) = \mu_s^0+\nu\overline{R_u}T\ln(\gamma_{m,s}^{\pm}m_s) \quad (29)$$

$$\mu_w(T,p) = \mu_w^0+\overline{R_u}T\ln(a_w) \quad (30)$$

In Eqs. (29) and (30), the symbols "ν", "$\mu^{0''}$, "γ" and "a_w" refer to dissociation number (3) for $CaCl_2$ (Rard and Clegg, 1997)), standard chemical potential, the activity coefficient, and the activity of water in the solution and "m" and "s" subscripts denote mean ionic and solute material, respectively. The conversion of solution mass concentration (C) to its corresponding molality (m) executed via Eq. (31);

$$m = \frac{C}{(1-C)}\times\frac{1}{M_s} \quad (31)$$

For determining the value of physical exergy, it is customary to select the temperature and pressure of ambient as dead state conditions. For determining the exergy of humid airflow saturated state of outdoor air is commonly chosen as a dead state (Wang et al., 2010). The selected dead state for liquid desiccant should be consistent with that of humid air. Water is the limitation of the ultimate diluted solution, so the ultimate dead state of liquid desiccant is selected at ambient temperature (T_0), ambient pressure (p_0), and solution concentration of *0* % or equivalently $x_s\rightarrow 0$ and $x_w\rightarrow 1$ according to Eqs. (33) and (34), respectively. The ultimate diluted solution, which is denoted by subscript "*0,s*" in Eq. (25), is a theoretical limitation, and for engineering calculations, the $x_{0,s}$ value of 0.0001 has been used. After some manipulation, the molar fraction could be converted to molality via Eq. (32); by this equation, the dead state molar fraction of 0.0001 would be equivalent to 0.0056 mol/kg. Also, the dead state temperature and humidity ratio of humid air are taken to be 30 °C and 0.0271 kg/kg, respectively.

$$m = \frac{x_s}{(1-x_s)}\times\frac{1}{M_w} \quad (32)$$

$$\mu_{0,s} = \lim_{x_s\rightarrow 0}\mu_s(T_0,p_0,x_s) \quad (33)$$

$$\mu_{0,w} = \lim_{x_w\rightarrow 1}\mu_w(T_0,p_0,x_w) \quad (34)$$

In Eq. (25), the numerical value of standard chemical potential (μ^0) for solute and water in third and fourth parentheses does not matter and does not influence the value of desiccant exergy. Also, the numerical values of mean molal ionic activity coefficient, "γ" and water activity in solution, "a_w" depend on the solution molality and are obtained from Ref. (Rard and Clegg, 1997).

Exergy destruction is a scale of irreversibility measurement in any process, and its value in steady adiabatic systems could be determined using the inlet/outlet exergy flow rates to/from the system (X_i and X_o in Eq. (35), respectively)

$$X_{des} = \sum X_i - \sum X_o \quad (35)$$

For example, for the dehumidifier system the exergy destruction rate could be evaluated using Eq. (36);

$$\dot{X}_{des} = (\dot{X}_{t,sol,i}+\dot{X}_{a,i})-(\dot{X}_{t,sol,o}+\dot{X}_{a,o}) \quad (36)$$

Having the exergy flow rates of air and desiccant streams, the 2nd law efficiency of *H/M* exchanger could also be evaluated by dividing the outlet exergy flow to inlet one according to Eq. (37);

$$\eta_{2^{nd}} = 1-\frac{X_{des}}{X_i} = \frac{(X_{t,sol,o}+X_{a,o})}{(X_{t,sol,i}+X_{a,i})} \quad (37)$$

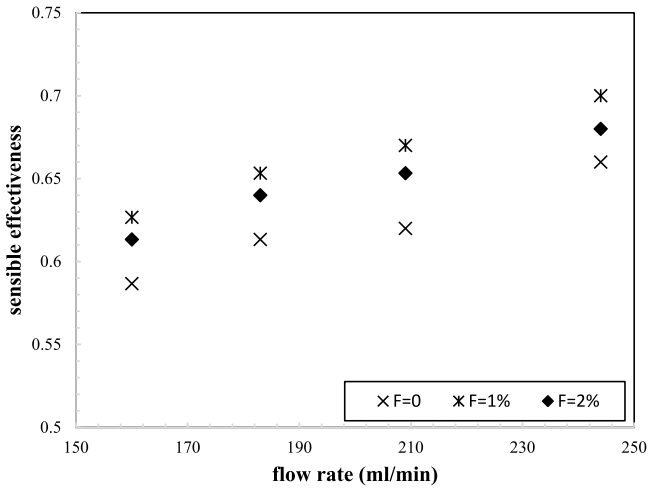

Fig. 4. The variation of sensible effectiveness vs. the solution flow rate for 20 °C inlet solution temperature and different NP concentrations.

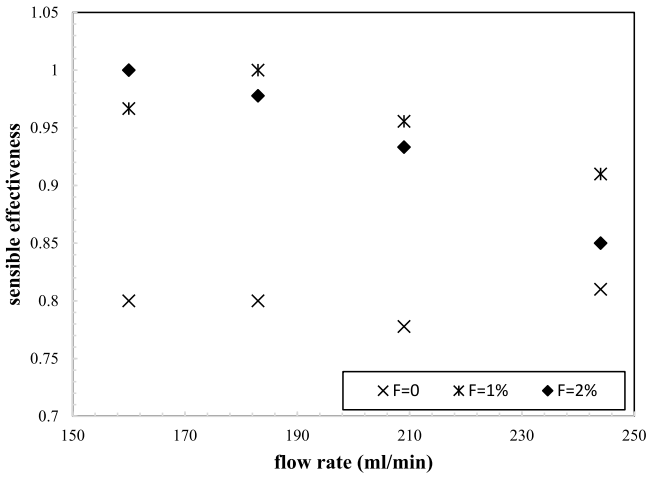

Fig. 5. The variation of sensible effectiveness vs. the solution flow rate for 26 °C inlet solution temperature and different NP concentrations.

4. Uncertainty analysis

Every experimental work is accompanied by a certain value of uncertainty; for directly measured parameters, the uncertainty is the sensitivity of measuring devices and for calculated quantities, the uncertainty is calculated considering their relation to measured parameters through a mathematical relation. In this work, the uncertainty values of effectiveness, *SHF*, and 2nd law efficiency are determined using the uncertainty propagation method whose relation is given by Eq. (38) (Coleman et al., 2010).

$$Z = f(X_1, X_2, X_3, \ldots)$$
$$\delta Z = \sqrt{\left(\frac{\partial Z}{\partial X_1}\delta X_1\right)^2 + \left(\frac{\partial Z}{\partial X_2}\delta X_2\right)^2 + \left(\frac{\partial Z}{\partial X_3}\delta X_3\right)^2 + \cdots} \quad (38)$$

In Eq. (38), the uncertainty of calculated parameter Z is denoted by δZ, which depends on directly measured properties of X_1, X_2, X_3, etc. The maximum values of the uncertainties involved in this study are summarized in Table 3.

5. Results and discussion

5.1. Energy analysis

In the following sections, the energy exchanger analyzed using the energy rating parameters including the *SHF* and effectiveness values of the system. The sensitivity analysis is performed to unveil the effects of solution flow rate, inlet temperature, and the NP concentrations according to values given in Table 2.

5.1.1. Sensible effectiveness

In sensible effectiveness equation (Eq. (8), for each case of solution temperature, the value of the denominator is the same through the experiments, and therefore, the diagram of ϵ_s shows mainly the sensible heat transfer variation. The variation of sensible effectiveness versus the solution flow rate in cases of 20 °C and 26 °C inlet solution temperatures are depicted in Figs. 4 and 5, respectively.

By inspecting the variation of sensible effectiveness in Figs. 4 and 5 it is revealed that for pure desiccant solution (0% concentration) at both solution temperatures, the sensible effectiveness increased by the solution flow rate increment from 160 ml/min to 244 ml/min; by growing the solution flow rate in this range, the sensible effectiveness improved by 15.8% and 8.4% in cases of 20 °C and 26 °C inlet solution temperatures, respectively. This result is due to the enhancement of the heat transfer coefficient by the solution flow rate increase. Also, the improving effect of the solution flow rate increase on sensible effectiveness is more prominent for lower solution temperature, which is due to the higher solution to air temperature difference in this case. By inspecting the sensible effectiveness variation against the solution flow rate, the following statements could be made;

- Using *NF* instead of a pure desiccant solution, the sensible effectiveness improved at all studied solution flow rates. For the inlet solution temperature of 20 °C, using 2% *NF* instead of the pure solution the sensible effectiveness improved by 4.4% and 4% at flow rates of 160 ml/min and 244 ml/min, respectively; the corresponding values for 26 °C solution temperature are 25% and 5%, respectively.
- In the case of using the *NF* desiccant solution of 26 °C temperature, the overall variation of sensible effectiveness vs. the solution flow rate is decreasing. In this case, by the solution flow rate increase from 160 ml/min to 244 ml/min, the sensible effectiveness reduced by 9% and 17% for *NF* concentrations of 2% and 1%, respectively. This behavior shows the reducing effect of flow rate increment by using *NF* desiccant solution (Bejan, 2016). In adiabatic exchanger systems, the moisture absorption by desiccant and the resulted in liberated heat of phase change gives rise to a temperature increase of both air and desiccant solution. By the higher heat transfer coefficient in the solution side (Bejan, 2016), its temperature grows more, and this eventually leads to the increase of mean temperature difference between desiccant and the airflow streams. This demonstrates again the highest improving effect of using *NF* desiccant solution which is at low solution flow rates and high temperatures.

Considering the importance of heat capacitance ratio (Cr^*) as one of the influencing factors that affect the sensible effectiveness, the variation of ϵ_s vs. Cr^* for 20 °C and 26 °C inlet solution temperatures are depicted in Fig. 6 and Fig. 7, respectively. by using 0% desiccant solution, although the variation trend of sensible effectiveness vs. the solution flow rate is increasing in both solution temperatures, the change rate for lower solution temperature (20 °C) is higher; in this case, by increasing the Cr^* from 2.9 to 4.3, the sensible effectiveness grows by 12.4% and 1.2% for 20 °C and 26 °C solution temperatures, respectively. Another point which could be inferred from Figs. 6 and 7 is that for each

Table 3
The maximum uncertainty of parameters studied in this work.

Experimental parameters	*Unit*	*Uncertainty value*
Measured parameters	T_{db} (°C)	*0.2*
	T_{wb} (°C)	*0.2*
	T_{sol} (°C)	*0.2*
	V_{sol} (CC)	*5*
	m_{sol} (gr)	*0.001*
	t (s)	*1*
	$\dot{V}_a$ ($\frac{m^3}{s}$)	*0.5*
	$\dot{V}_{sol}$ ($\frac{ml}{s}$)	*0.05*
	C_{sol}	*0.001*
Calculated parameters	*HR(gr/kg)*	*0.04*
	Cr_*	*0.13*
	R	*0.05*
	ϵ_s	*0.003*
	ϵ_l	*0.003*
	ϵ_t	*0.002*
	LMTD (°C)	*0.25*
	SHF	*0.004*
	X_{des} (W)	*0.004*
	η_2^{nd}	*0.008*

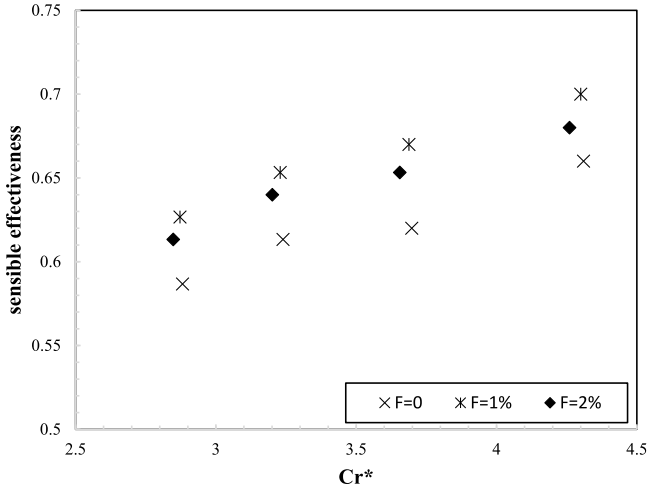

Fig. 6. The variation of sensible effectiveness vs. Cr^* for 20 °C solution temperature and different *NP* concentrations.

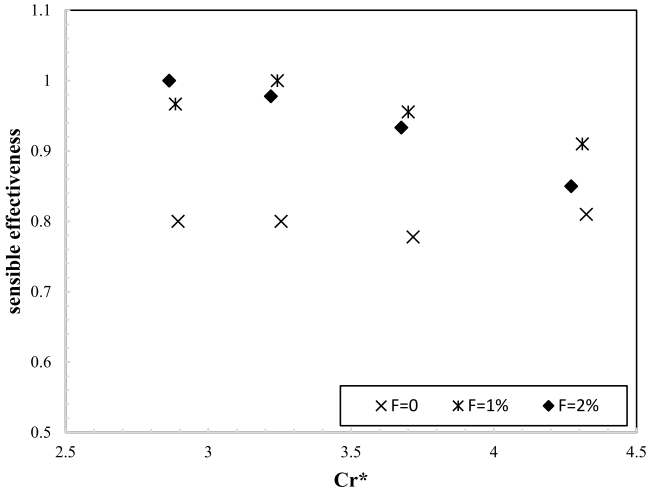

Fig. 7. The variation of sensible effectiveness vs. the Cr^* for 26 °C solution temperature and different *NP* concentrations.

solution flow rate, the value of Cr^* is different in cases of different *NP* concentrations; at each solution flow rate by increasing the *NP* concentration, the Cr^* is reduced accordingly. As mentioned earlier, having a constant airflow rate, the value of NTU_s, and the overall heat sensible transfer (U_s) remain fixed through the experiments, and hence the only parameter affected by changing the solution flow rate is Cr^*.

5.1.2. Latent effectiveness

The variations of latent effectiveness vs. the solution flow rate for inlet solution temperatures of 20 °C and 26 °C are depicted in Fig. 8 and Fig. 9, respectively.

The equilibrium vapor pressure is a function of solution temperature and concentration. In this way, as the denominator of Eq. (14) depends on thermodynamics properties of inlet air and solution streams and from the uniqueness of these properties throughout the experiments (except in cases of different inlet solution temperatures and *NP* concentrations) the variation of latent effectiveness in Figs. 8 and 9 shows that of the *MRR*. Also, although the presence of *NP* reduces the equilibrium vapor pressure and by Eq. (14) decreases the latent effectiveness, but this change is not very large and is at the utmost 6.4%. The prevailing trend observed is that the latent effectiveness increased

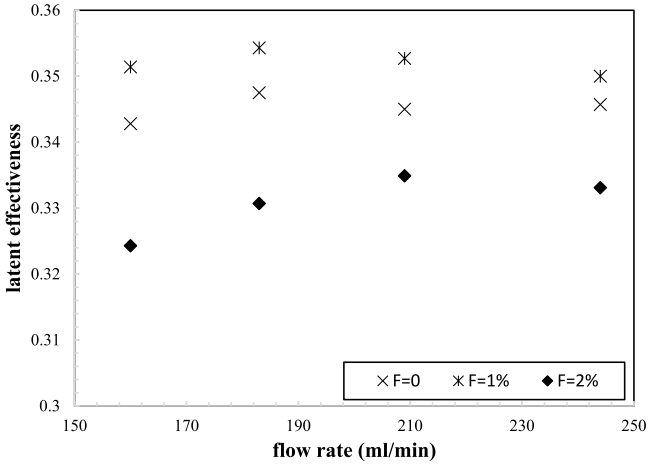

Fig. 8. The variation of latent effectiveness vs. the solution flow rate for 20 °C solution temperature and different NP concentrations.

by the solution flow rate increase. By increasing the solution flow rate from 160 ml/min to 244 ml/min, the average latent

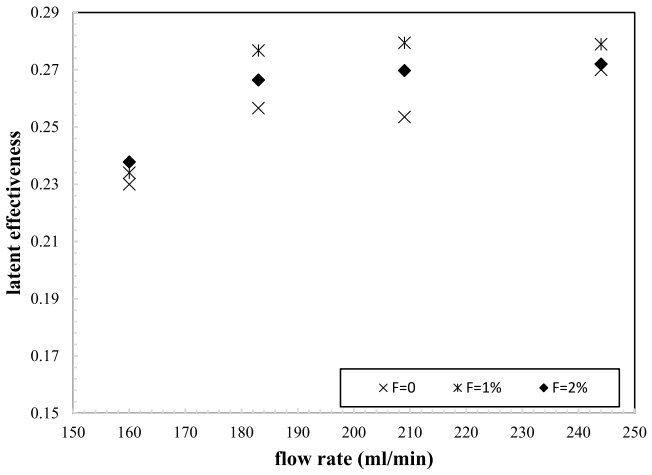

Fig. 9. The variation of latent effectiveness vs. the solution flow rate for 26 °C solution temperature and different *NP* concentrations.

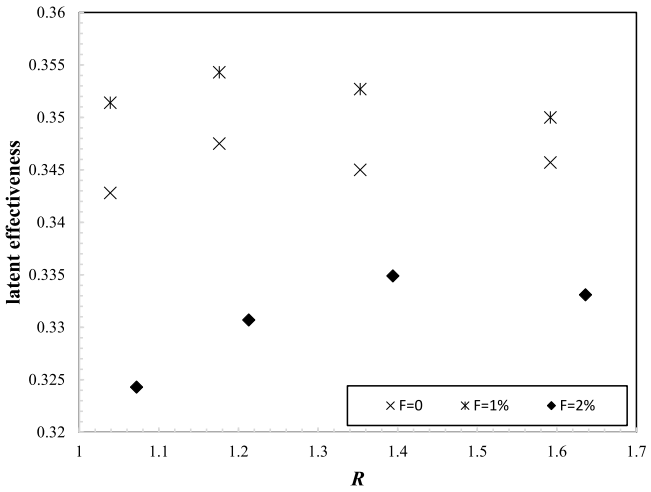

Fig. 10. The variation of latent effectiveness vs. the solution flow rate ratio for 20 °C inlet solution temperature and different NP concentrations.

effectiveness increased by 1% and 17% in cases of 20 °C and 26 °C solution temperatures, respectively. This shows the relatively greater importance of the solution flow rate on mass transfer enhancement in high solution flow rates. Also, by using *NF* of 1% concentration instead of a pure solution, the latent effectiveness grows at all solution flow rates. The mass transfer enhancement resulted from using the *NF* instead of pure desiccant could be attributed to improving mechanisms of hydrodynamics and grazing effects. The *NP* diameter is smaller than membrane pores, and under the effect of Brownian motion and turbulence, the particles penetrate the membrane surface and remain there temporarily. By the vapor adsorption to *NP*s surface and under the action of Brownian motion, they go back to the liquid bulk flow and release the gas molecules there. Next, the NPs are regenerated, after which this cycle is repeated and enhances the moisture transfer. On the other hand, the presence of the *NP*s would affect the hydrodynamic properties of the desiccant and improves gas transmission. This mechanism, which could be named boundary layer mixing, is the result of particle collision to each other due to Brownian motion in the gas–liquid interface. This would eventually alleviate the concentration boundary layer thickness and decreases resistance against moisture transfer (Wen et al., 2018a). Also, the existence of *NP*s affects the turbulence and gives rise to the renewal of the liquid film, and improves the mass transfer over the membrane surface (Hajilary and Rezakazemi, 2018). By comparing the effects of using *NF* in place of the pure desiccant solution on sensible (Fig. 4 and Fig. 5) and latent (Figs. 8 and 9) effectiveness, the following statements could be made;

- In the case of 26 °C inlet solution temperature, using *NF* instead of a pure desiccant solution, the sensible and latent effectiveness are both enhanced. The improvement of sensible effectiveness is larger in low solution flow rates and becomes smaller at higher flow rates. Also, between the sensible and latent effectiveness, the larger enhancement effect of using *NF* is for sensible effectiveness; while the average increment of latent effectiveness in the case of 2% *NP* concentration is 3.5%, the corresponding value for sensible effectiveness is 18%. This shows the higher improving effect of using *NF* solution on heat transfer rather than mass transfer which is more dominant at higher solution temperature.
- In the case of using 20 °C solution temperature, although by using *NF* solution the sensible effectiveness is improved at all solution flow rates and *NP* concentrations the situation for latent effectiveness is not the same; while using a desiccant solution of 1% *NP* concentration instead of pure solution enhances latent effectiveness, using 2% concentration solution attenuate it. As a result of using a solution of 2% particle concentration, the average values of sensible and latent effectiveness improved and declined by 4%, respectively.
- Using a 1% *NF* solution always improves the sensible and latent effectiveness. In other words, increasing the NP concentration from a specific value has not the improving effect at all conditions and, in some cases, may even have a reverse effect on system performance.

The variation of latent effectiveness vs. the flow rate ratio (R) for 20 °C and 26 °C solution temperatures are depicted in Fig. 10 and Fig. 11, respectively. Although the overall variations of ϵ_l versus the solution flow rate and flow rate ratio (R) are nearly the same the values of R, are different for different *NF* concentrations. The change of R-value by changing the *NP* concentration is due to density change as denoted by Eq. (12), whose effect is revealed in desiccant mass flow rate (Eq. (11)).

5.1.3. Total effectiveness

The variations of total effectiveness vs. the solution flow rate in the case of 20 °C and 26 °C inlet solution temperatures are depicted in Fig. 12 and Fig. 13, respectively.

By inspecting the trends observed in Figs. 12 and 13, the following results could be obtained;

- Although for lower inlet solution temperature (20 °C), the overall variation of total effectiveness for all *NF* concentrations vs. the solution flow rate is increasing, for higher (26 °C) solution temperature, a common trend is not observed. In the case of using pure desiccant, by increasing the solution flow rate from 160 ml/min to 244 ml/min, the total effectiveness grown by 4.7% and 5% for 20 °C and 26 °C inlet solution temperatures, respectively. By using the *NF* desiccant solution, in the case of 20 °C inlet solution temperature, a positive change of ϵ_T by the solution flow rate increase was observed, but the trend is increasing–decreasing for 26 °C temperature. From the dependence of total effectiveness to sensible and latent effectiveness (Eq. (23)), different trends observed in variation of ϵ_T for 26 °C inlet solution temperature could be attributed to the

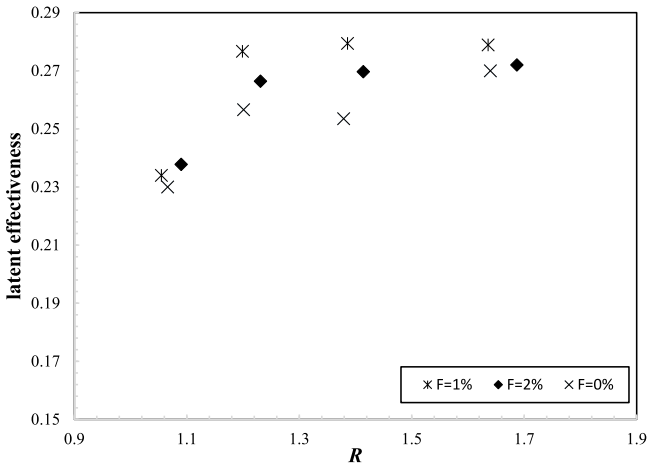

Fig. 11. The variation of latent effectiveness vs. the solution flow rate ratio for 26 °C inlet solution temperature and different NP concentrations.

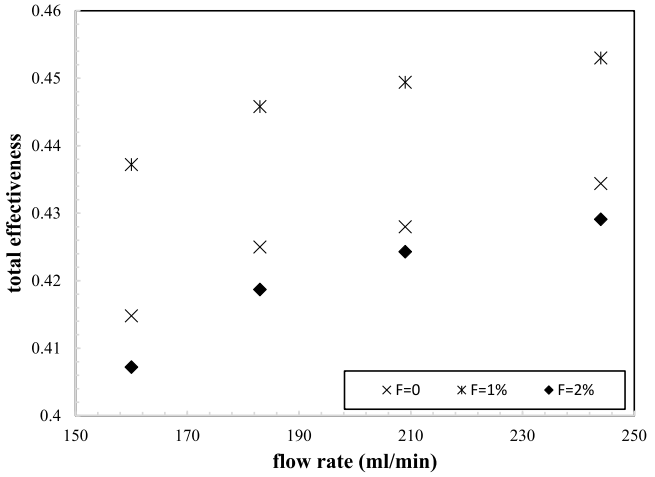

Fig. 12. The variation of total effectiveness vs. the solution flow rate for 20 °C inlet solution temperature and different NP concentrations.

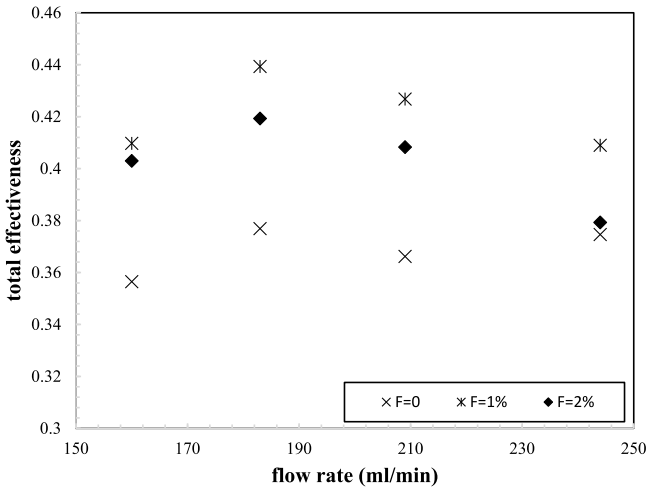

Fig. 13. The variation of total effectiveness vs. the solution flow rate for 26 °C inlet solution temperature and different NP concentrations.

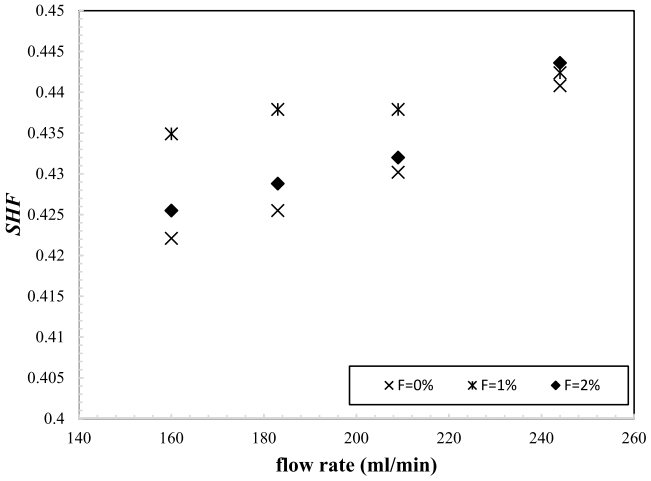

Fig. 14. The variation of *SHF* vs. the solution flow rate for 20 °C inlet solution temperature and different NP concentrations.

unusual decrease of sensible effectiveness by the solution flow rate increase (Fig. 7).

- Using *NF* of 1% concentration in place of the pure desiccant solution, the value of total effectiveness improved at all solution flow rates and inlet temperatures. The mean improvement made by using 1% *NF* instead of the pure desiccant solution is 4.9% and 14.3% in cases of 20 °C and 26 °C inlet solution temperatures, respectively. This suggests the biggest improvement of total energy transfer is for the highest solution temperature (26 °C) and 1% *NP* concentration.

5.2. Sensible heat factor (SHF)

The variation of sensible heat factor against the solution flow rate in cases of 20 °C and 26 °C solution temperatures are depicted in Fig. 14 and Fig. 15, respectively. The overall variation of *SHF* for two solution temperatures are different; while the value of *SHF* increased by the solution flow rate for 20 °C solution temperature, it is alleviated for 26 °C solution temperature. Using pure desiccant (0% *NP* concentration), by increasing the solution flow rate from 160 ml/min to 244 ml/min, the *SHF* value increased and decreased by 4.4% and 14.9% for 20 °C and 26 °C solution temperatures, respectively. The different effects of the solution flow rate increase on *SHF* could be attributed to different effects of solution flow rate on heat and moisture transfer coefficients of desiccant solution. Although both values of heat and mass transfer coefficients increased by growing the solution flowrate but for the higher solution temperature (i.e., 26 °C), the mass transfer and for lower solution temperature (i.e., 20 °C) the heat transfer coefficient increased more. This would eventually lead to *SHF* decrease and increase by the solution flow rate increment in cases of 26 °C and 20 °C temperatures, respectively.

By comparing the *SHF* values for 20 °C and 26 °C solution temperatures, it is apparent that for each solution flow rate, the *SHF* is lower in the former cases. Also, the respective decreasing and increasing trend observed vs. the solution flow rate gives rise to converging and finally equality of the *SHF* at high solution flow rates; at maximum solution flow rate of 244ml/min at the *SHF* would be reached to 0.44. This shows that the major effect of using NP on *SHF* is in low solution flow rates and diminishes by enlarging the solution flow rate.

About the influence of *NP* addition on *SHF*, it is inferred that, particularly in low solution flow rates using *NF* instead of the pure desiccant solution increases the value of *SHF*. At a solution

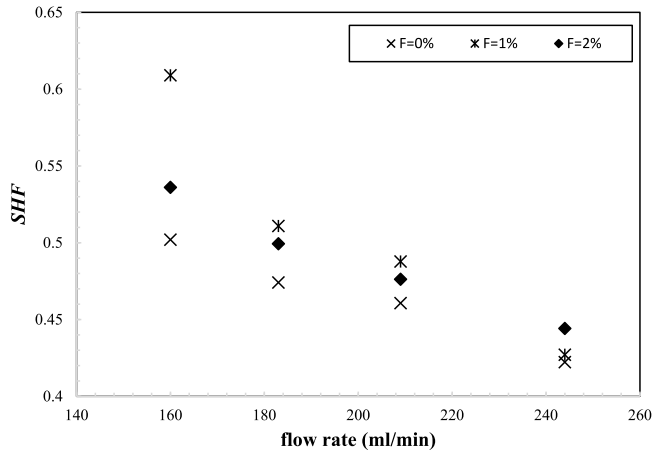

Fig. 15. The variation of *SHF* vs. the solution flow rate for 26 °C inlet solution temperature and different NP concentrations.

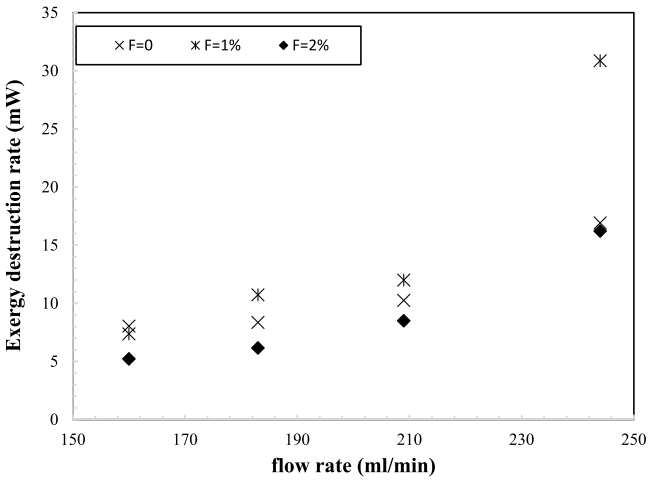

Fig. 16. The rate of exergy destruction vs. the solution flow rate for 20 °C inlet solution temperature and different NP concentrations.

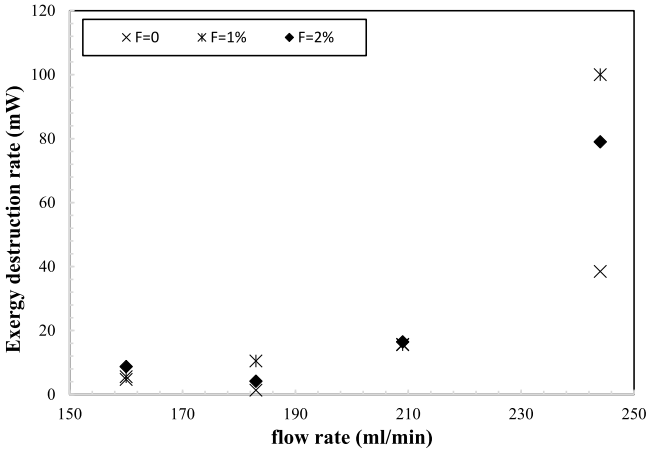

Fig. 17. The rate of exergy destruction vs. the solution flow rate for 26 °C solution temperature and different NP concentrations.

flow rate of 160 ml/min by using 1% *NF* instead of pure desiccant, the *SHF* value increased by 3% and 21% for solution temperatures of 20 °C and 26 °C, respectively. The improving mechanisms of convective heat and mass transfer coefficients are similar; in this way, through both two coefficients increased by adding NPs, the increasing trend of *SHF* resulted by adding NP shows the more extensive effect of the heat transfer rather than mass transfer enhancement. Also, by increasing *NP* concentration, the portion of latent heat increased accordingly; by using 2% instead of 1% *NF* solution, the *SHF* value decreased by 2.2% and 12% in cases of 20 °C and 26 °C inlet solution temperatures respectively. This section could be concluded that the sensitivity of *SHF* value against solution flow rate, temperature, and particle concentration is more at conditions of 1% *NP* concentration, higher temperature (26 °C), and lower solution flow rates.

5.3. Exergy analysis

The exergy analysis of the system could be performed by presenting either the rate of exergy destruction (Eq. (36)) or 2nd law efficiency (Eq. (37)). The rate of exergy destruction vs. the solution flow rate in cases of 20 °C and 26 °C inlet solution temperature is depicted in Fig. 16 and Fig. 17, respectively.

As demonstrated in Figs. 16 and 17, the overall variation of exergy destruction by the flow rate for both solution temperatures is increasing. When using 1% *NF* desiccant solution, by the flow rate increase from 160 ml/min to 244 ml/min the rate of exergy destruction increased 3.19 and 10.44 folds for 20 °C and 26 °C solution temperatures; the corresponding values for 2% *NF* concentration are 2.11 and 8.03 times, respectively. This could be attributed to the growing heat and mass transfer resulted from the solution flow rate increase. Also, the largest exergy destruction is for 1% *NF* solution, which is from the highest rate of *HMT* for this case between the other study cases. Another result which could be drawn from the variation observed in Figs. 16 and 17 is the small sensitivity of destroyed exergy to both solution flow rate and *NP* concentration which is more evident for solution flow rates below 210 ml/min; in this region, the maximum variation of exergy destruction rate due to the change of solution flow rate is less than 63% and 200% in cases of 20 °C and 26 °C inlet solution flow rates, respectively. The maximum change of exergy destruction rate resulted from using *NF* desiccant instead of the pure desiccant solution took place at the highest flow rate (244 ml/min) which is for 1% *NF* solution. By using 1% *NF* desiccant, the rate of exergy destruction increased by 82% and 167% in the case of 20 °C and 26 °C inlet solution temperatures. The difference between the rates of exergy destruction at two solution temperatures is throughout the solution flow rates but became higher at larger solution flow rates. By using a desiccant solution of 26 °C instead of 20 °C, the rate of exergy destruction enlarged 3.9, 2.2, and 1.27 times for *NF* concentrations of 0% (having no particles), 1%, and 2%, respectively. This shows the great effect of NP presence in the exergy performance of the system, especially at high values of *NP* concentration and inlet solution temperatures. The increasing effect of *NF* solution temperature and concentration on exergy destruction rate resulted in a reduction of 2nd law efficiency. The variation of 2nd law efficiency of system vs. solution flow rate for 20 °C and 26 °C inlet solution temperatures are outlined in Figs. 18 and 19, respectively. By Eq. (37), the exergy destruction rate has the reverse effect on the value of 2nd law efficiency and as it was expected, the cases with the highest rate of exergy destruction have the lowest values of 2nd law efficiency and vice versa. At maximum solution flow rate of 244 ml/min by using *NF* solution of 1% instead of pure (0%) one the 2nd law efficiency decreased by 5% and 11.3% for 20 °C and 26 °C solution temperatures.

5.4. The standard deviation

For each calculated parameter the standard deviation in its corrected sample is calculated according to Eq. (39). In Eq. (39), x

Table 4
The values of standard deviation for the involved parameters in different working conditions.

	$T = 20$ °C			$T = 26$ °C		
	0%	1%	2%	0%	1%	2%
ε_s	0.039	0.015	0.040	0.038	0.089	0.041
ε_l	0.002	0.005	0.003	0.025	0.042	0.014
ε_T	0.009	0.015	0.017	0.009	0.015	0.017
SHF	0.008	0.003	0.008	0.033	0.076	0.039
X_{des} (mW)	0.004	0.013	0.004	0.036	0.014	0.048
η_{2nd} (%)	0.570	3.456	1.045	6.983	3.201	8.006

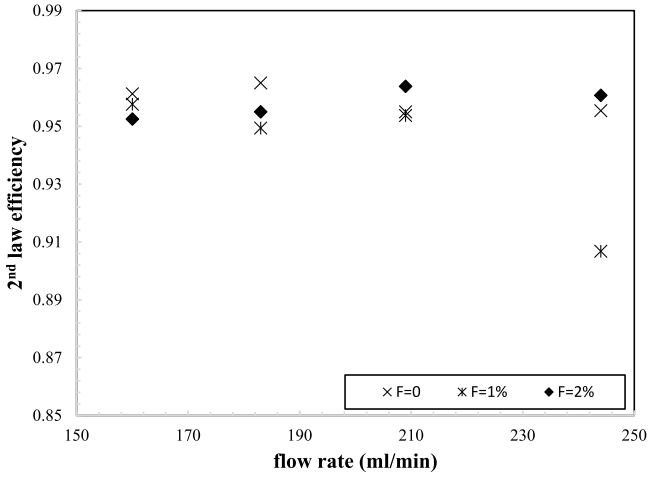

Fig. 18. The variation of 2nd law efficiency vs. the solution flow rate for 20 °C solution temperature and different *NP* concentrations.

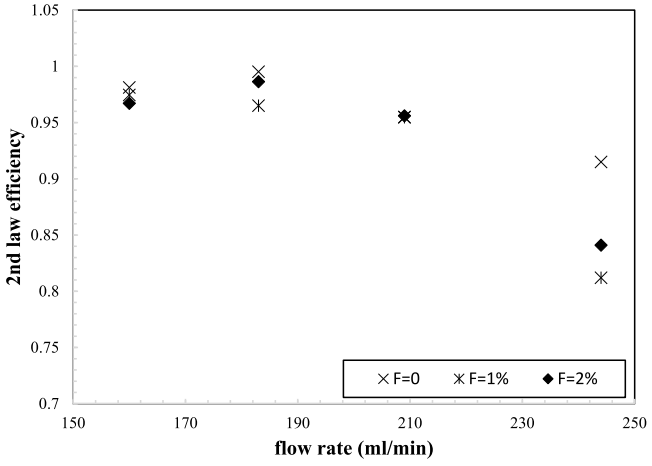

Fig. 19. The variation of 2nd law efficiency vs. the solution flow rate for 26 °C solution temperature and different *NP* concentrations.

represents the calculated parameter, $\bar{x}$ is the mean value and n is the number of samples (Ghasemi et al., 2020; Orooji et al., 2020; Hassandoost et al., 2019; Karimi-Maleh et al., 2021; Gholami et al., 2019),

$$SD = \sqrt{\frac{\sum(x_i - \bar{x})^2}{n - 1}} \tag{39}$$

The values of standard deviation for the involved parameters are listed in Table 4. As could be seen, the standard deviation of the involved parameters is very small compared to their corresponding values; also, the values of standard deviation for 26 °C solution temperature is higher than the corresponding values for 20 °C solution temperature.

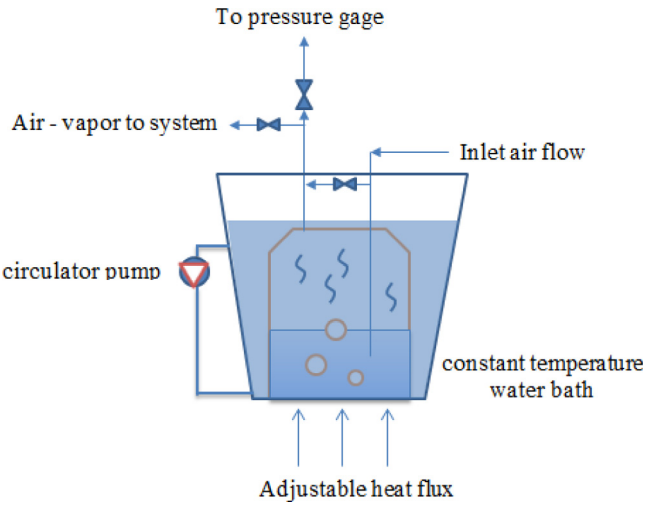

Fig. A.1. The schematic of the air humidifier system.

6. Conclusion

The air dehumidification by aqueous $SiO_2/CaCl_2$ *NF* desiccant solution in a membrane-based *LDAC* system has been investigated experimentally. The setup system is a hollow fiber membrane energy exchanger (*HFMEE*) where the air flows through the fibers and desiccant flows over them. By studying the system performance in different working conditions of *NF* concentrations, solution temperatures, and flow rates, the following statements could be drawn;

- By using *NF* instead of the pure desiccant solution, the sensible effectiveness grows at all solution flow rates and temperatures. The mean change of sensible effectiveness resulted by using 2% *NF* instead of pure desiccant is 18% and 4% in cases of 20 °C and 26 °C solution temperatures which shows the higher improvement of sensible effectiveness in the condition of lower solution temperatures.
- Using NF in place of pure desiccant does not improve the latent effectiveness in all working conditions. For 26°C solution temperature using 1% and 2% NF solution, the mean value of latent effectiveness altered by +6% and +3.5% while the corresponding values for 20 °C solution are +2% and -4%, respectively. This suggests the highest improving effect is for the case of a 1% *NF* solution.
- Using 1% *NF* instead of the pure desiccant solution, the value of total effectiveness is improved at all solution flow rates and temperatures. The highest improvement of total energy transfer was observed in solution temperature 26 °C and *NF* solution 1%.
- The prevailing effect of using *NF* in place of the pure desiccant solution on the value of *SHF* is increasing. Using 1% *NF* in place of pure desiccant, the *SHF* growth would be the highest. Also, the greatest effect of using *NF* on *SHF* is

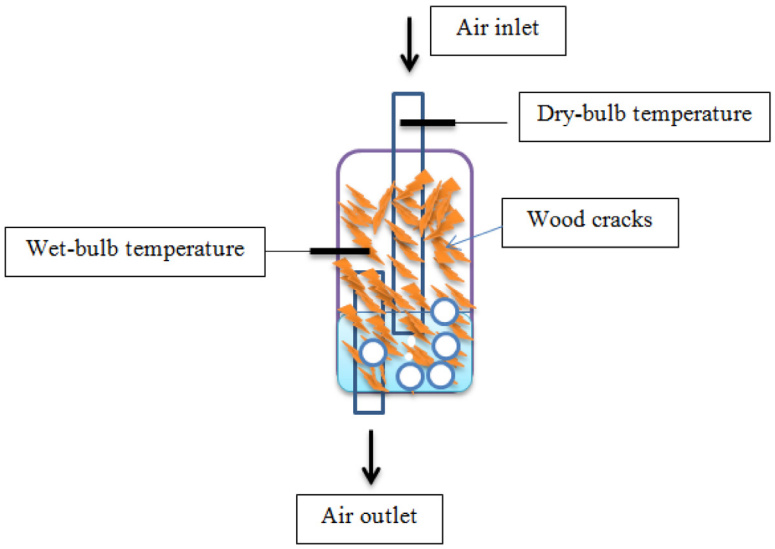

Fig. A.2. The handmade experimental psychrometer.

at conditions of 26 °C solution temperature and the lowest flow rates.

– The second law analysis shows that using *NF* instead of the pure desiccant solution deteriorates the exergetic performance of the system, but the degree of exergy destruction is not directly proportional to the *NP* concentration. The highest rate of exergy destruction is for the desiccant solution of 1% *NP* and 26 °C temperature and the lowest is for a pure desiccant solution.

CRediT authorship contribution statement

Yaping Wang: Methodology, Software, Validation, Writing - review & editing, Investigation. **Behrooz Ruhani:** Methodology, Software, Validation, Writing - review & editing, Investigation. **Mohammad Ali Fazilati:** Methodology, Software, Validation, Writing - original draft, Investigation. **S. Mohammad Sajadi:** Methodology, Software, Validation, Investigation. **As'ad Alizadeh:** Methodology, Software, Validation, Investigation. **Davood Toghraie:** Methodology, Software, Validation, Writing - original draft, Investigation.

Declaration of competing interest

The authors declare that they have no known competing financial interests or personal relationships that could have appeared to influence the work reported in this paper.

Appendix

The air humidifier is of the bubble-type whose components and its flow paths are shown schematically in Fig. A.1. If the air temperature was below the specified set value, a variable voltage power source turns on the electric wire heater which raises the air temperature to the specified value.

For determining the air properties a handmade psychrometer was used whose schematic is shown in Fig. A.2.

After connecting the airflow to the exchanger and from the pressure loss in its way through the fibers, its flow rate would be decreased, and the air temperature and humidity ratio deviate from the preset values. Therefore, before directing the air stream into the fibers, an equivalent pressure loss was exerted to airflow to provide the correct air properties when it was connected to the module. The equivalent external pressure drop was applied by a thermally insulted set valve (Fig. A.3). The values of the wet bulb and dry bulb temperatures of air (T_{wb} and T_{db} in Fig. A.3) are adjusted in a way that makes the required air properties of inlet airflow using the isenthalpic property of the valve. After getting the specified properties, the air canal disconnected from the set valve and connected to the module, and simultaneously the solution pump turned on and data acquisition triggered.

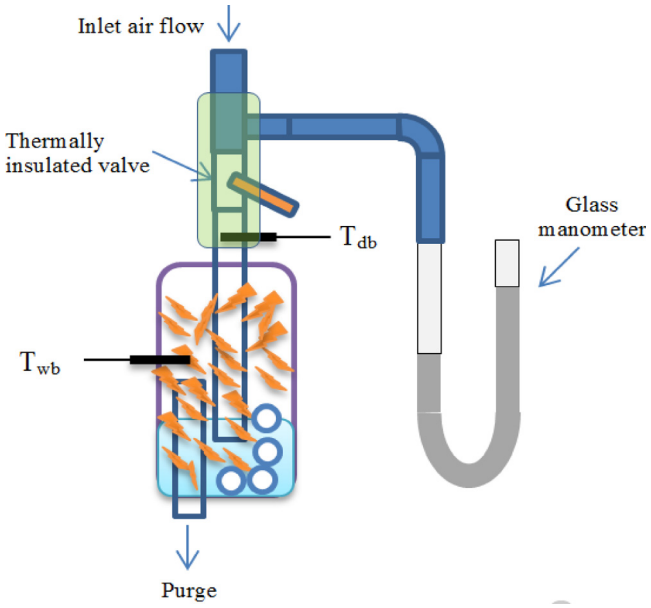

Fig. A.3. Adjusting the air properties using the set valve before starting the experiment.

References

Abdel-Salam, A.H., Simonson, C.J., 2016. State-of-the-art in liquid desiccant air conditioning equipment and systems. Renew. Sustain. Energy Rev. 58, 1152–1183.

AHRI A, 2005. Standard for Rating Air-To-Air Exchangers for Energy Recovery Ventilation Equipment. Air-Conditioning & Refrigeration Institute, Arlington, VA, Book Standard for Rating Air-to-Air Exchangers for Energy Recovery Ventilation Equipment, Air-Conditioning & Refrigeration Institute, Series

Standard for Rating Air-to-Air Exchangers for Energy Recovery Ventilation Equipment, Air-Conditioning & Refrigeration Institute.
Ali, A., Vafai, K., Khaled, A.R., 2003. Comparative study between parallel and counter flow configurations between air and falling film desiccant in the presence of nanoparticle suspensions. Int. J. Energy Res. 27 (8), 725–745.
Bejan, A., 2016. Advanced Engineering Thermodynamics. John Wiley & Sons.
Coleman, H.W., Steele, W.G., Buzhuga, M., 2010. Experimentation validation and uncertainty analysis for engineers. Noise Control Eng. J. 58 (3), 343–344.
Conde, M.R., 2004. Properties of aqueous solutions of lithium and calcium chlorides: formulations for use in air conditioning equipment design. Int. J. Therm. Sci. 43 (4), 367–382.
Dong, C., Lu, L., Qi, R., 2017a. Model development of heat/mass transfer for internally cooled dehumidifier concerning liquid film shrinkage shape and contact angles. Build. Environ. 114, 11–22.
Dong, C., Lu, L., Wen, T., 2017b. Experimental study on dehumidification performance enhancement by TiO2 superhydrophilic coating for liquid desiccant plate dehumidifiers. Build. Environ. 124, 219–231.
Fazilati, M.A., Sedaghat, A., Alemrajabi, A.A., 2016. Natural induced flow due to concentration gradient in a liquid desiccant air dehumidifier. Appl. Therm. Eng. 105, 105–117.
Fazilati, M.A., Sedaghat, A., Alemrajabi, A.-A., 2017. Transient performance and temperature field of a natural convection air dehumidifier loop. Heat Mass Transf. 53 (7), 2287–2296.
Ghasemi, M., Khataee, A., Gholami, P., Soltani, R.D.C., Hassani, A., Orooji, Y., 2020. In-situ electro-generation and activation of hydrogen peroxide using a CuFeNLDH-CNTs modified graphite cathode for degradation of cefazolin. J. Environ. Manag. 267, 110629. http://dx.doi.org/10.1016/j.jenvman.2020.110629.
Gholami, P., Dinpazhoh, L., Khataee, A., Orooji, Y., 2019. Sonocatalytic activity of biochar-supported ZnO nanorods in degradation of gemifloxacin: Synergy study, effect of parameters and phytotoxicity evaluation. Ultrason. Sonochem. 55, 44–56. http://dx.doi.org/10.1016/j.ultsonch.2019.03.001.
Hajilary, N., Rezakazemi, M., 2018. CFD modeling of CO2 capture by water-based nanofluids using hollow fiber membrane contactor. Int. J. Greenhouse Gas Control 77, 88–95.
Hassandoost, R., Pouran, S.R., Khataee, A., Orooji, Y., Joo, S.W., 2019. Hierarchically structured ternary heterojunctions based on Ce^{3+} / Ce^{4+} modified Fe_3O_4 nanoparticles anchored onto graphene oxide sheets as magnetic visible-light-active photocatalysts for decontamination of oxytetracycline. J. Hazard. Mater. 376, 200–211. http://dx.doi.org/10.1016/j.jhazmat.2019.05.035.
Huang, Y., Niu, J-l., Chung, T-m., 2012. Energy and carbon emission payback analysis for energy-efficient retrofitting in buildings—Overhang shading option. Energy Build. 44, 94–103.
Karimi-Maleh, H., Ranjbari, S., Tanhaei, B., Ayati, A., Orooji, Y., Alizadeh, M., Karimi, F., Salmanpour, S., Rouhi, J., Sillanpää, M., Sen, F., 2021. Novel 1-Butyl-3-methylimidazolium bromide impregnated chitosan hydrogel beads nanostructure as an efficient nanobio-adsorbent for cationic dye removal: Kinetic study. Environ. Res. 195, 110809. http://dx.doi.org/10.1016/j.envres.2021.110809.
Kim, H., Jeong, J., Kang, Y.T., 2012. Heat and mass transfer enhancement for falling film absorption process by SiO2 binary nanofluids. Int. J. Refrig. 35 (3), 645–651.
Kotas, T.J., 2013. The Exergy Method of Thermal Plant Analysis. Elsevier.
Lin, S.J.F., Shigang, Z., 2011. Experimental study on vertical vapor absorption into libr solution with and without additive. Appl. Therm. Eng. 31 (14–15), 2850–2854.
Liu, Y., Wei, Y., Su, J., Zhang, L., Cui, X., Jin, L., 2020. Surface-modified PVA/PVDF hollow fiber composite membrane for air dehumidification. J. Mater. Sci. 55 (13), 5415–5430.
Liu, J., Zhang, T., Liu, X., Jiang, J., 2015. Experimental analysis of an internally-cooled/heated liquid desiccant dehumidifier/regenerator made of thermally conductive plastic. Energy Build. 99, 75–86.
Nanomaterials, U., 2018. US Research Nanomaterials, Inc, The advanced nanomaterials provider. US Research Nanomaterials.
Orooji, Y., Ghanbari, M., Amiri, O., Salavati-Niasari, M., 2020. Facile fabrication of silver iodide/graphitic carbon nitride nanocomposites by notable photocatalytic performance through sunlight and antimicrobial activity. J. Hazard. Mater. 389, 122079. http://dx.doi.org/10.1016/j.jhazmat.2020.122079.
Pak, B.C., Cho, Y.I., 1998. Hydrodynamic and heat transfer study of dispersed fluids with submicron metallic oxide particles. Exp. Heat Transfer Int. J. 11 (2), 151–170.
Pang, C., Lee, J.W., Kang, Y.T., 2015. Review on combined heat and mass transfer characteristics in nanofluids. Int. J. Therm. Sci. 87, 49–67.
Pitzer, K.S., 1995. Thermodynamics. McGraw-Hill College.
Qi, R., Dong, C., Zhang, L.-Z., 2020. A review of liquid desiccant air dehumidification: From system to material manipulations. Energy Build. 215, 109897.
Rard, J.A., Clegg, S.L., 1997. Critical evaluation of the thermodynamic properties of aqueous calcium chloride. 1. Osmotic and activity coefficients of 0-10.77 mol ⊙ kg-1 aqueous calcium chloride solutions at 298.15 K and correlation with extended pitzer ion-interaction models. J. Chem. Eng. Data 42 (5), 819–849.
Shadanfar, H., Elhambakhsh, A., Keshavarz, P., 2021. Air dehumidification using various TEG based nano solvents in hollow fiber membrane contactors. Heat Mass Transf. 1–9.
Tso, C.Y., Chao, C.Y., 2015. Study of enthalpy of evaporation, saturated vapor pressure and evaporation rate of aqueous nanofluids. Int. J. Heat Mass Transfer 84, 931–941.
Wang, L., Li, N., Zhao, B., 2010. Exergy performance and thermodynamic properties of the ideal liquid desiccant dehumidification system. Energy Build. 42 (12), 2437–2444.
Wen, T., Lu, L., 2019. Numerical and experimental study on internally cooled liquid desiccant dehumidification concerning film shrinkage shape and vapor condensation. Int. J. Therm. Sci. 136, 316–327.
Wen, T., Lu, L., Dong, C., Luo, Y., 2018a. Investigation on the regeneration performance of liquid desiccant by adding surfactant PVP-K30. Int. J. Heat Mass Transfer 123, 445–454.
Wen, T., Lu, L., Li, M., Zhong, H., 2018b. Comparative study of the regeneration characteristics of LiCl and a new mixed liquid desiccant solution. Energy 163, 992–1005.
Wen, T., Lu, L., Zhong, H., 2018c. Investigation on the dehumidification performance of LiCl/H2O-MWNTs nanofluid in a falling film dehumidifier. Build. Environ. 139, 8–16.
Xiong, Z., Dai, Y., Wang, R., 2010. Development of a novel two-stage liquid desiccant dehumidification system assisted by CaCl2 solution using exergy analysis method. Appl. Energy 87 (5), 1495–1504.
Xuan, Y., Li, Q., 2000. Heat transfer enhancement of nanofluids. Int. J. Heat Fluid Flow 21 (1), 58–64.
Xuan, Y., Roetzel, W., 2000. Conceptions for heat transfer correlation of nanofluids. Int. J. Heat Mass Transfer 43 (19), 3701–3707.
Yan, S.-R., Fazilati, M.A., Boushehri, R., Mehryaar, E., Toghraie, D., Nguyen, Q., et al., 2020. Experimental analysis of a new generation of membrane liquid desiccant air-conditioning (LDAC) system with free convection of desiccant for energy economic management. J. Energy Storage 29, 101448.
Yulin Ma, M.A.F., Sedaghat, Ahmad, Toghraie, Davood, Talebizadehsardari, Pouyan, 2020. Natural convection energy recovery loop analysis, Part I: Energy and exergy studies by varying inlet air flow rate. Heat Mass Transf. 56, 1685–1695.
Zhang, L., Liu, X., Jiang, J., Jiang, Y., 2014. Exergy calculation and analysis of a dehumidification system using liquid desiccant. Energy Build. 69, 318–328.
Zhu, B.J., Zhao, W.L., Li, J.K., Guan, Y.X., Li, D.D., 2011. Thermophysical properties of Al2O3-water nanofluids. In: Conference Thermophysical Properties of Al2O3-Water. Nanofluids. 688, pp. 266–271.